

# Personalisation of a Cardiac Electrophysiology Model using Optical Mapping and MRI for Prediction of Changes with Pacing

Jatin Relan, Mihaela Pop, Hervé Delingette\*,  
Graham Wright, Nicholas Ayache and Maxime Sermesant

**Abstract**—Computer models of cardiac Electrophysiology (EP) can be a very efficient tool to better understand the mechanisms of arrhythmias. Quantitative adjustment of such models to experimental data (personalisation) is needed in order to test their realism and predictive power, but it remains challenging at the organ scale. In this paper, we propose a framework for the personalisation of a 3D cardiac EP model, the Mitchell-Schaeffer (MS) model, and evaluate its volumetric predictive power under various pacing scenarios. The personalisation was performed on *ex-vivo* large porcine healthy hearts using Diffusion Tensor MRI (DT-MRI) and optical mapping data. The MS Model was simulated on a 3D mesh incorporating local fibre orientations, built from DT-MRI. The 3D model parameters were optimised using features such as 2D epicardial depolarisation and repolarisation maps, extracted from the optical mapping. We also evaluated the sensitivity of our personalisation framework to different pacing locations and showed results on its robustness. Further, we evaluated volumetric model predictions for various epi- and endocardial pacing scenarios. We demonstrated promising results with a mean personalisation error around 5 ms and a mean prediction error around 10 ms (5 % of the total depolarisation time). Finally, we discussed the potential translation of such work to clinical data and pathological hearts.

## I. INTRODUCTION

Modelling cardiac electrophysiology *in silico* has been an important research topic for the last decades [1]–[4], and it can be a very efficient tool to better understand the mechanisms of arrhythmias. Personalisation of such models to experimental data is needed in order to test their realism and predictive power, but remains difficult at the scale of the organ. Personalisation is defined as the estimation of model parameters which best fit simulations to data. In this paper, we propose a robust personalisation method for a volumetric cardiac electrophysiology model using surface data and we test its predictive power. The personalisation and prediction evaluation were

done using the high quality *ex-vivo* electrophysiology data obtained from the fusion of optical and MR imaging.

Cardiac electrophysiology models of the myocyte Action Potential (AP) at cellular and sub-cellular scales can be broadly classified into three main categories: Ionic Models (IM), Phenomenological Models (PM) and Eikonal Models (EM). IM [1], [2], [4]–[6] characterise ionic currents flowing through the cardiac cell membrane with varying complexity and accuracy and have many parameters and variables (it can be more than 50). Most of them are computationally expensive to simulate in volumetric domains and not well suited to solve inverse problems (parameter estimation). EM [3], [7], [8] are very simple, describing only the time at which a depolarisation wave reaches a given point without precisely modelling the potential value. At the intermediate level are PM [9]–[11], which describe and capture just the shape of action potential generation and propagation along the cell membrane, without modelling all the ionic currents.

Here, we personalised a simplified biophysical model, the Mitchell-Schaeffer (MS) model [12], modelling the action potential as a combination of sodium ( $\text{Na}^+$ ), calcium ( $\text{Ca}^{2+}$ ) and potassium ( $\text{K}^+$ ) phenomenological ionic currents. We chose this model because of the following reasons: (i) it provides a good analytical understanding of the membrane dynamics, (ii) it has a limited number of parameters (5) to estimate, (iii) each parameter has a simple physical interpretation, and (iv) it has explicit analytical formulae to express most of the measured features and restitution properties using model parameters [12]. Finally, it was compared to another classical PM models (the Aliev-Panfilov model [10]), and the MS model was providing a better fit (lower final error, especially for the APD) with a more homogeneous parameter map for conductivity [13].

In this paper, the cardiac electrical activity was acquired *ex-vivo* from controlled experiments using optical imaging of the epicardium of healthy porcine hearts [14]. The optical signal directly represents the tissue action potential. This data was then processed to extract features of the AP propagation such as depolarisation time (DT), repolarisation time (RT), Conduction Velocity (CV), Action Potential Duration (APD) and their restitutions. These features were then fused with a volumetric mesh created from MRI of the *ex-vivo* hearts, to obtain epicardial surface data.

Electrophysiology model personalisation can be basically addressed as an inverse problem of parameter estimation. This

Manuscript received July 29, 2010; revised October 26, 2010. *Asterisk indicates corresponding author - email: herve.delingette@inria.fr.*

J. Relan, H. Delingette, N. Ayache and M. Sermesant are with INRIA, Asclepius research project, Sophia Antipolis, France

M. Pop and G. A. Wright are with the University of Toronto, Dept. of Medical Biophysics, Sunnybrook Health Sciences Centre, Canada

M. Sermesant is also with the King's College London, Division of Imaging Sciences, St. Thomas Hospital, United Kingdom.

This paper has supplementary downloadable material available at <http://ieeexplore.ieee.org>, provided by the authors. This includes three multimedia AVI format movie clips, which show personalisation and prediction videos.

Copyright (c) 2010 IEEE. Personal use of this material is permitted. However, permission to use this material for any other purposes must be obtained from the IEEE by sending an email to [pubs-permissions@ieee.org](mailto:pubs-permissions@ieee.org).

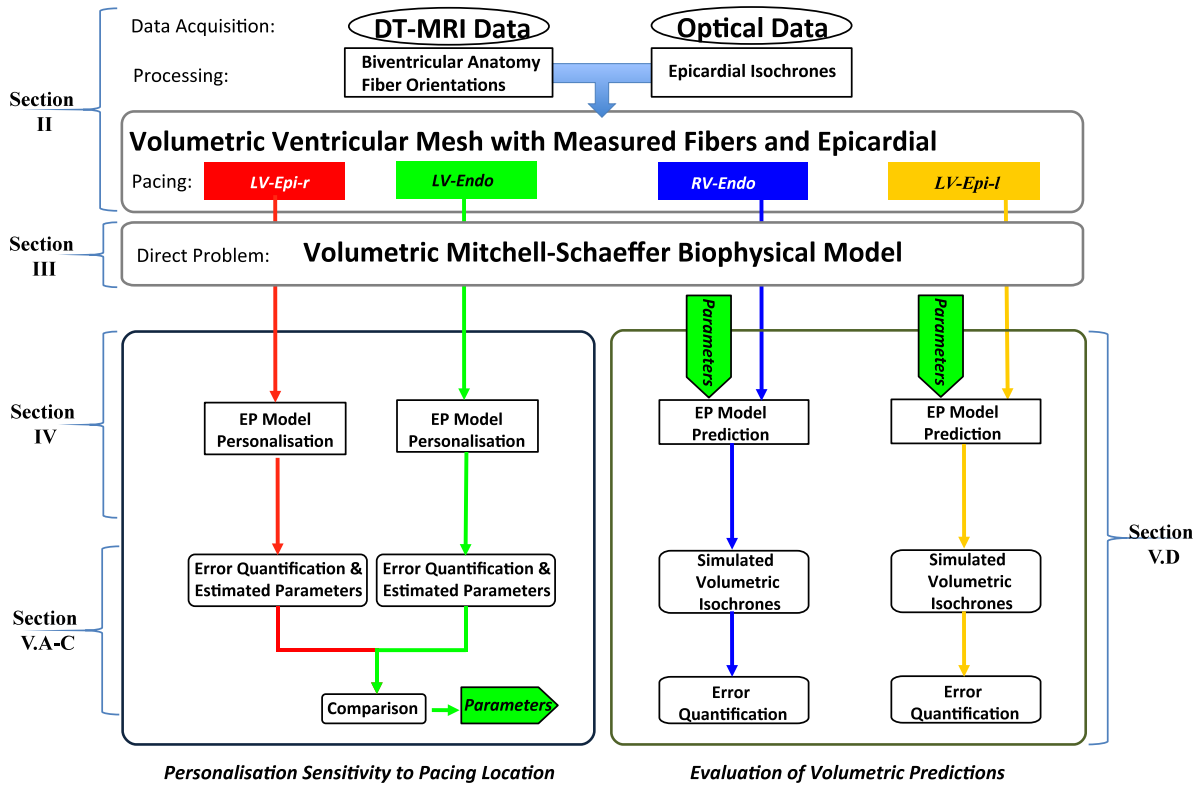


Fig. 1. Flowchart describing the outline of this paper.

problem was first addressed using a single heart cycle for 2D phenomenological Aliev & Panfilov model in [15], where the AP propagation was simulated on a simple surface mesh modelling a dog's heart epicardium. Only the model parameter for the DT feature was adjusted. It was also performed for 2D EM in [16] again with adjustment of the same feature but for patient data. Finally, initial step towards personalisation of the 3D Aliev & Panfilov model were taken in [17] with adjustment of DT and APD features from a single cycle.

In this paper, we propose a personalisation framework for a 3D macroscopic MS model on a volumetric bi-ventricular mesh of the myocardium using 2D epicardial surface data. The robustness of this method to different pacing locations and its predictive power were assessed.

## II. DATA ACQUISITION AND PROCESSING

The experimental data acquired consist of epicardial optical imaging that records the AP wave propagation, and Diffusion Tensor-MRI representing the anatomy and fibre orientations. The optical data have a higher spatial resolution compared to *in-vivo* mapping data and provides a direct measurement of the AP [18]. Such dense and controlled data enabled the validation of the personalisation method and prediction results. The data was acquired and processed in three stages (see Fig 2):

### Stage 1: Optical Imaging Data

The explanted heart was attached to a Langendorff perfusion system with fluorescence dye and the electro-mechanical uncoupler (to suppress heart motion) injected into the perfusion

line. More details of the experimental setup can be found elsewhere [14]. The heart was paced at a given rate, with an electrode near the apex with a square wave voltage stimulus of 2-4V for 5 ms. The fluorescence signals were captured with high temporal (270 fps) and spatial ( $< 1mm$ ) resolution, using a pair of CCD cameras. Lastly, 5-7 opaque markers were glued onto the epicardium and imaged, so as to provide a way to register the optical images with the epicardial surface of the model generated from MRI volume. Recorded 2D optical movie represents the changes in the fluorescent signal intensity, which follow the changes in the AP. The signal intensity was then analysed for each pixel of the movie to get DT and RT isochrones in the following way. First, the signal was scaled for each pixel between its baseline and maximum value, cropping under the baseline which we got from segmenting the values into two clusters, the baseline being defined as the mean value of the lowest cluster. The scaled recordings were then filtered with a 3D Gaussian convolution, spatially isotropic with a kernel width of 1.0 and temporally using a kernel width of 3.0.

The DT were detected using the zero crossing of the second ( $d^2F/dt^2$ ) derivatives of the fluorescence signal intensity  $F$  (Fig 2(b)). The RT were detected using  $APD_{90}$  (APD at 90% repolarisation, which is 0.9 times the difference between the action potential peak amplitude and the baseline (Fig 2(b))). Finally, the DT isochrones and APD maps for each cycle were reconstructed as 2D images (Fig 2(c & d)).

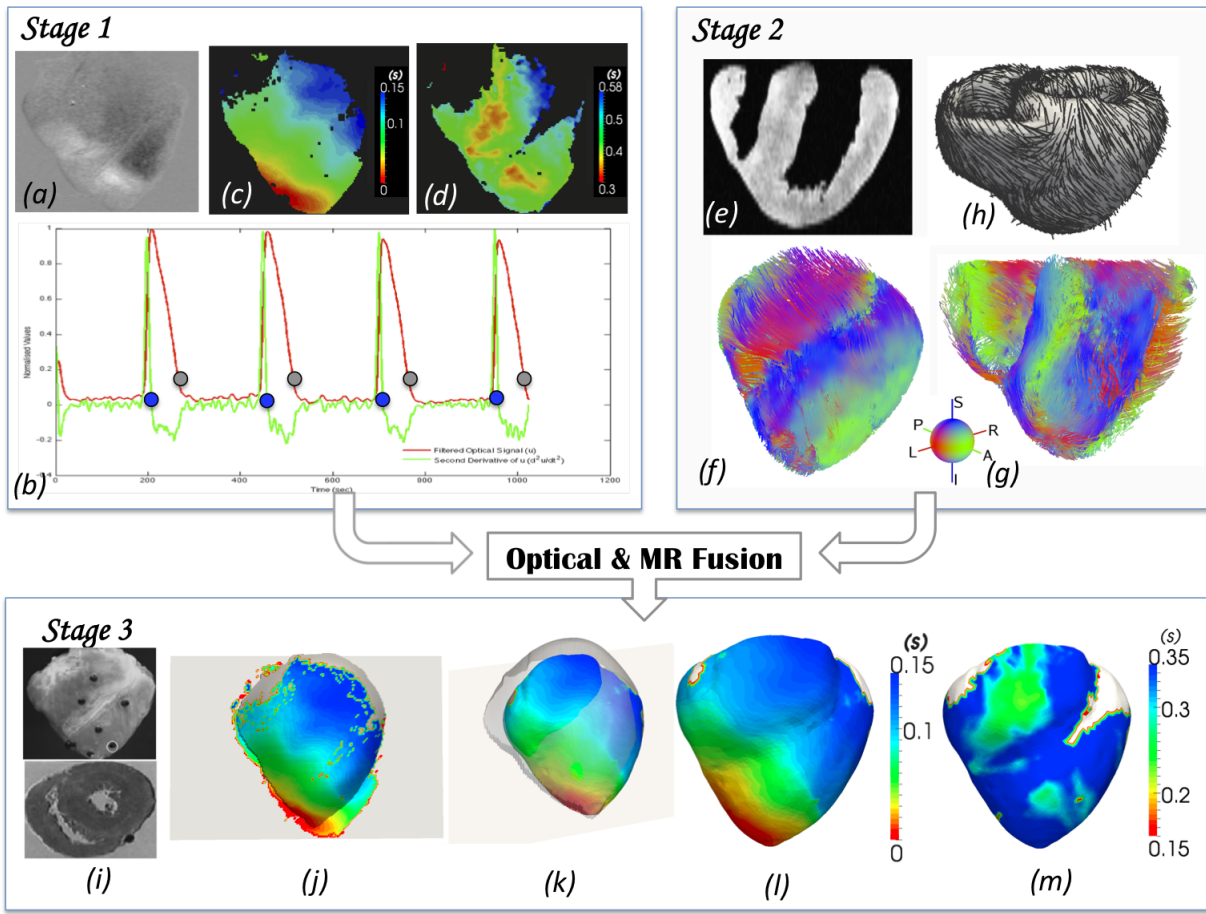


Fig. 2. *Stage 1* (a) Raw optical data acquired (antero-lateral view). (b) Extraction of depolarisation times (blue dots) and  $APD_{0}$  (gray dots), (c) & (d) Extracted DT & APD isochronal maps. *Stage 2* (e) DT-MRI slice, (f) & (g) Fibre tracking from DT-MRI, (h) Volumetric mesh with assigned fibre orientations. *Stage 3* (i) top: A snapshot showing the epicardial markers using optical camera, bottom: MRI slice showing markers, (j) Stereoscopic surface generated from the two optical CCD cameras with extracted features, (k) Registration of stereoscopic surface to the volumetric mesh using markers and features projection, (l) & (m) Resulting DT and APD maps on the mesh for epicardial surface only.

### Stage 2: Diffusion Tensor-MRI Data

The hearts were then imaged using a MR scanner. The details on MR pulse sequences and setup used is described in details in [14]. An in-plane resolution of  $0.5 \times 0.5 \text{mm}^2$  and slice thickness of 1.5 mm was used. The heart anatomy was extracted from the MR data using classical segmentation algorithms such as thresholding, mathematical morphology, isosurface extraction, and used to generate a volumetric tetrahedral mesh using CGAL (<http://www.cgal.org>) and GHS3D (TetMesh, <http://www.distene.com>) software. For each vertex, the assigned fibre direction is the principal eigenvector of the corresponding voxel in the reconstructed tensor image, see Fig 2(h).

### Stage 3: Optical and MR Data Fusion

The optical images recorded by the two CCD cameras were used to reconstruct the 3D surface of the heart using stereoscopy (Fig 2(i)) [19]. The 2D isochronal maps generated were then rectified based on the cameras calibration and stereoscopic parameters. Each pixel of the isochronal maps corresponds to a vertex on the grid mesh of the stereoscopic surface (Fig 2(j)). The glued opaque markers were imaged

with optical as well as MR data. An affine registration of the stereoscopic surface onto the volumetric mesh was then performed using these markers [14] (Fig 2(i)).

The DT isochrones and APD maps for each cycle were projected onto the volumetric mesh with an interpolation from the triangular stereoscopic surface, resulting in epicardial DT isochrones and APD maps on the bi-ventricular mesh (Fig 2(k-m)).

### Dataset Used for Personalisation

We used two *ex-vivo* hearts, which were optically imaged for steady-state heart cycles and scanned with DT-MRI. The first heart was paced to produce 4 different optical datasets, all at a frequency of 1.1 Hz, but obtained using 4 different pacing locations (Fig 3(1st, 2nd, 3rd & 4th column)) which were near the apex of:

- *1A-LV-Epi-l*: left ventricle epicardium (left side).
- *1B-LV-Epi-r*: left ventricle epicardium (right side).
- *1C-LV-Endo*: left ventricle endocardium.
- *1D-RV-Endo*: right ventricle endocardium.

The second heart was paced to produce 5 different optical datasets, all paced at one location near the apex of the left

## Epicardial Surface Data

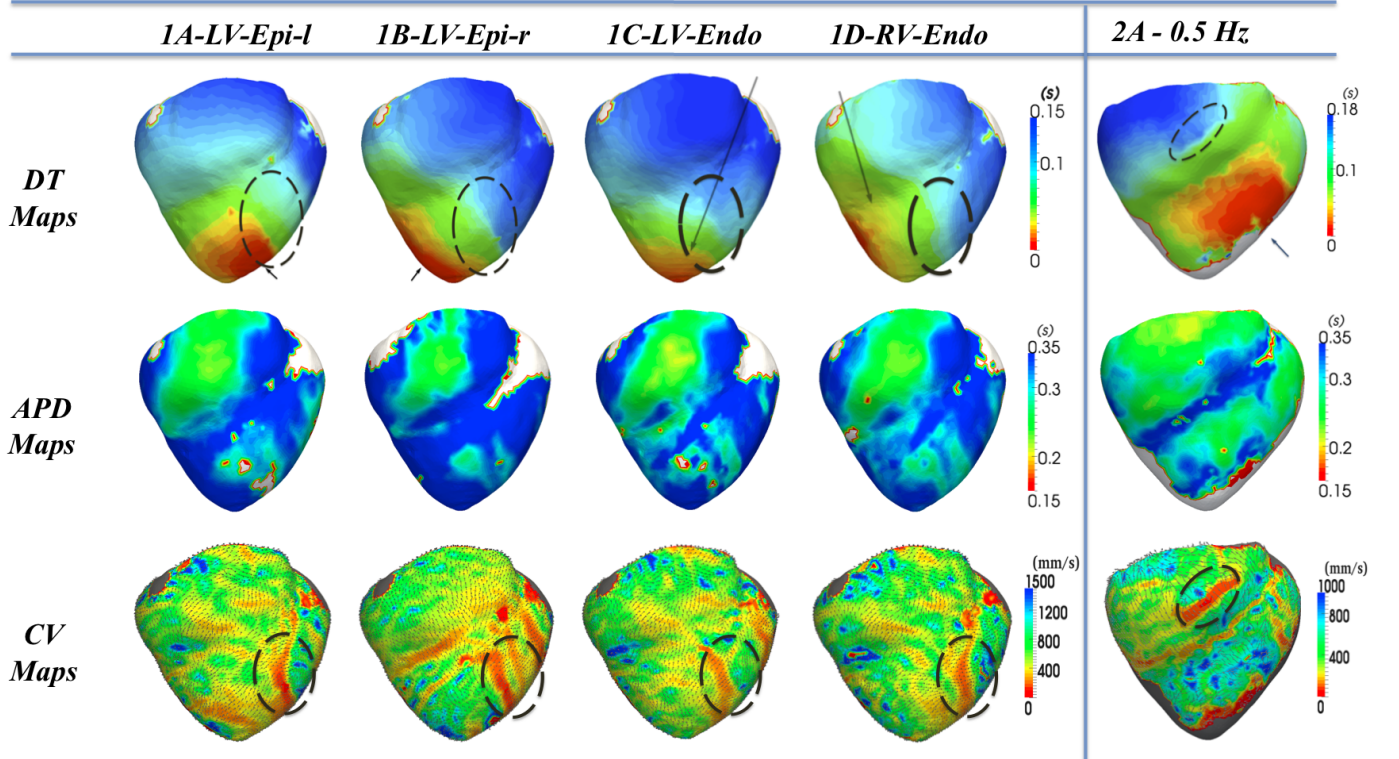


Fig. 3. The first four columns are for dataset 1 and the last column is for dataset 2. The first row shows the measured epicardial DT isochrones for various pacing locations (depicted by arrows), the second row shows the respective APD maps and the third row shows the local  $CV^{msd}$  computed from the measured DT isochrones (small arrows on the surface show CV direction). Black ellipses highlight the regions having low conductivity.

ventricle epicardium, but for 5 different Pacing Frequency (PF) (Fig 3(5th column)): 0.5 Hz (2A), 0.7 Hz (2B), 0.9 Hz (2C), 1.1 Hz (2D), 1.2 Hz (2E).

Although these were healthy hearts, we could identify discrete areas of low conductivity (see black ellipse in Fig 3). This was most likely due to tissue becoming ischemic around a small branch of blood vessel, partially occluded by an air bubble accidentally trapped into the perfusion line, resulting in oxygen deprivation of the tissue and further installation of acute ischemia and cellular uncoupling. As a result, an altered morphology of action potentials accompanied by a lowering of CV was observed in these areas.

### III. MODEL SIMULATION: DIRECT PROBLEM

The MS model [12] is a 2-current simplified biophysical model derived from the 3-current ionic Fenton Karma model [20]. The MS model is described by the following system of Partial Differential Equations (PDE)

$$\begin{cases} \partial_t u = \text{div}(D\nabla u) + \frac{zu^2(1-u)}{\tau_{in}} - \frac{u}{\tau_{out}} + J_{stim}(t) \\ \partial_t z = \begin{cases} \frac{(1-z)}{\tau_{open}} & \text{if } u < u_{gate} \\ \frac{-z}{\tau_{close}} & \text{if } u > u_{gate} \end{cases} \end{cases} \quad (1)$$

where,  $u$  is the normalised action potential variable, and  $z$  is the gating variable, which makes the gate open and close, thus depicting the depolarisation and repolarisation phase.  $J_{in} = (zu^2(1-u))/\tau_{in}$  represents combination of all inward

phenomenological ionic currents, primarily  $Na^+$  &  $Ca^{2+}$ , which raises the action potential voltage and  $J_{out} = -u/\tau_{out}$  represents combination of all outward phenomenological currents, primarily  $K^+$  that decreases the action potential voltage describing repolarisation.  $J_{stim}$  is the stimulation current, at the pacing location.

The parameters of the reaction terms and their standard values as reported in [12] are

- $\tau_{open}$ : opening time-constant of the gate = 0.120 s
- $\tau_{close}$ : closing time-constant of the gate = 0.150 s
- $\tau_{in}$ : time-constant for inward currents = 0.003 s
- $\tau_{out}$ : time-constant for outward currents = 0.06 s

The diffusion term in the model is controlled by the anisotropic  $3 \times 3$  Diffusion tensor  $D$  given by,  $D = d \cdot \text{diag}(1, r, r)$  in an orthonormal basis whose first vector is along the local fibre orientation, with  $d$  representing the cardiac tissue pseudo-conductivity in the fibre direction and  $r$  as the conductivity anisotropy ratio in the transverse plane. In order to have CV three times faster in the fibre direction than in the transverse plane [3], we fix a value of  $r = (1/3)^2 = 0.11$  (see Eq 2). Thus, we have only one parameter of the diffusion term and its standard value for  $CV = 50 \text{ cm/s}$  is given through a cardiac tissue pseudo-conductivity  $d = 1.5 \text{ s}^{-1}$ .

The model was spatially integrated on a 3D bi-ventricular tetrahedral mesh using a P1 Finite element method [21]. Using an appropriate discretisation in space for the model, with a mean edge length of  $\Delta x$ , leads to a system of

algebraic differential equations. The choice of  $\Delta x$  influences the numerical solution accuracy and depends on the maximum of  $du/dt$ . Thus we studied several time integration schemes (Explicit, Semi-Implicit and Implicit) for the model with respect to solution accuracy, stability and computational time expense (described in details in [13], [22]). As a result of this study, for MS model, we found the following optimum choice for spatial discretisation as  $\Delta x = 1.5mm$  and temporal discretisation as  $\Delta t = 0.1ms$ , with a semi-implicit, second order scheme known as Modified Crank-Nicolson/Adams-Bashforth (MCNAB) [22]. The model was simulated with initial pacing conditions as Dirichlet conditions (similar to voltage stimulus in experiments), where  $u$  and  $z$  value of 1 was imposed for certain duration to a set of vertices, which were chosen by extracting the earliest depolarising sites from the DT isochrones.

#### IV. MODEL PERSONALISATION: INVERSE PROBLEM

By model personalisation, we estimate the model parameters such that the model simulated features are similar to the extracted data features. Fortunately, MS model has this relationship defined explicitly for features like APD for a single cycle (see Eq 9) and APD & CV restitution (see Eq 11 and Eq 12). However CV for a single cycle is analytically defined in 1D using reaction-diffusion analysis [23] (see Eq 2), but in 3D, the wave front curvature also affects CV.

Using these relationships, we could determine the qualitative dependency of the extracted data features to the model parameters, see Table I.

	Single PF		Multiple PF	
	DT	APD	CV Rest.	APD Rest
$d$	✓	—	✓	—
$\tau_{in}$	✓	✓	✓	✓
$\tau_{out}$	—	✓	✓	✓
$\tau_{open}$	—	—	—	✓
$\tau_{close}$	—	✓	—	✓

TABLE I  
SENSITIVITY OF AP FEATURES TO MODEL PARAMETERS.

##### A. Case 1: Personalisation Using a Single PF

This case was applied to the first heart having a constant PF. In this case, we estimated the parameter  $d$  using DT isochrones and the parameter  $\tau_{close}$  using the APD, while all other parameters of the model were kept to their nominal values [12]. These adjustments are independent as there is no coupling between them (see Table I). Parameter estimation procedure is done as follows:

1) *Personalisation of DT Isochrones*: The apparent local CV ( $CV^{msd}$ ) of the epicardial tissue can be estimated from the spatial gradient of the measured DT isochrones  $T$  as,  $1/CV^{msd} = \|\nabla T_x\|$ . To avoid the amplification of the acquisition/fusion noise by the spatial derivatives, we smoothed  $CV^{msd}$  by averaging it over a neighbouring area, see Fig 3(3rd row). The analysis of the MS model for CV along the simulated wavefront has been studied in 1D [23] using travelling

wave train solutions and is found to be

$$CV^{sim} \propto \sqrt{\frac{d}{\tau_{in}}} \quad (2)$$

This relationship does not stand true in 3D propagation as the curvature of the wavefront affects  $CV^{sim}$ . Eq 2 shows one measured feature depending on two model parameters. We chose to estimate parameter  $d$  rather than  $\tau_{in}$ , which could be either estimated from restitution curves in case 2, or kept globally constant with a standard value in case 1. The estimation of parameter  $d$  was done in the following two steps:

a) *Calibration*: Here we initialise the model parameter  $d$  using the analytical relationship (see Eq 2). The calibration function used here was given by  $CV^{sim}(d) = \alpha\sqrt{d} + \beta$ , where the constants  $\alpha$  and  $\beta$  were to be determined for 3D model simulation.  $\alpha$  determines the scaling of Eq 2 in 3D with numerical diffusion and  $\beta$  was added to better fit the numerical simulations to Eq 2 and represents discretisation errors in 3D. The constants were determined by performing several model simulations for a range of  $d$  ( $d \in [0.1; 5.0]$ ) over the interval of stability of  $CV^{sim}(d) \approx 10cm/s - 2m/s$ . For each model simulation, a median of  $CV^{sim}(d)$  was computed. This gives rise to an overdetermined linear system given as

$$\begin{pmatrix} \vdots \\ medianCV_k^{sim}(d) \\ \vdots \end{pmatrix} = \begin{pmatrix} \vdots & \vdots \\ \sqrt{d_k} & 1 \\ \vdots & \vdots \end{pmatrix} \cdot \begin{pmatrix} \alpha \\ \beta \end{pmatrix} \quad (3)$$

where each line  $k$  is the result of a model simulation. The system (Eq 3) can also be written in matrix notation as,

$$medianCV^{sim} = \mathbb{D} \cdot \mathbb{P} \quad (4)$$

We solve Eq 4 in non-linear least squares sense by simply computing the pseudo-inverse:  $\mathbb{P} = (\mathbb{D} \cdot \mathbb{D}^T)^{-1} \cdot \mathbb{D}^T \cdot medianCV^{sim}$ . Once the relationship is estimated,  $d^{global}$  was determined from the median of  $CV^{msd}$  using

$$d^{global} = \left( \frac{medianCV^{msd} - \beta}{\alpha} \right)^2 \quad (5)$$

where  $medianCV^{msd} = median_{i \in S} (CV_i^{msd})$  with  $i$  the vertex index and  $S$  the set of the mesh vertices having measurements.

b) *Iterative adjustment*: This step was used to optimise the parameter  $d$  locally using a multi-resolution approach and the calibration result as initialisation. In order to start domain decomposition, we first divide the LV into 17 zones as defined by the American Heart Association (AHA), and similarly the RV into 9 zones. Then the zones with high cost function  $J(d_{zone})$  after optimisation were subdivided further into 4 zones for level I and so on (Fig 4).

The cost function for each zone was given as

$$J(d_{zone}) = \sum_{\forall i \in S \cap zone} (DT_i^{msd} - DT_i^{sim}(d_{zone}))^2 \quad (6)$$

with vertex  $i$  in zone, belonging to the surface  $S$  having measures. The cost function  $C_d$  for the myocardium was

$$C_d = \sqrt{\frac{1}{n} \sum_{\forall zone \in mesh \cap S} J(d_{zone})^2} \quad (7)$$

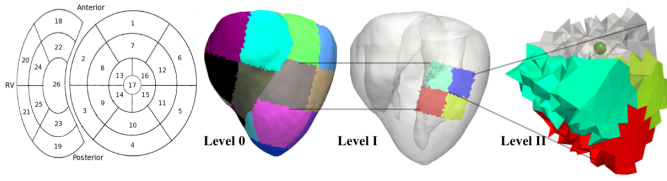


Fig. 4. Level 0 stands for the AHA segmentation of the bi-ventricular mesh into 26 zones. Level I is the subdivision of a zone into 4, Level II is a further subdivision. The green sphere is the zone barycentre.

where  $n$  is the number of zones having measured data. We minimise this cost function using trust region optimisation [24], which finds the minima of a subproblem such as a quadratic model created using the gradient and approximate Hessian matrix at the current search point implemented using Trilinos solver (<http://trilinos.sandia.gov>). The gradient is computed using a simple finite difference scheme given by

$$\frac{\partial J(d_{zone})}{\partial d} \approx \frac{J(d_{zone} + \Delta d) - J(d_{zone} - \Delta d)}{2\Delta d} \quad (8)$$

This optimisation was chosen to have a few number of gradient computations as they are computationally expensive and require two simulation steps.

When using domain decomposition, we obtain piecewise constant parameter maps. In order to have smooth parameter maps over the myocardium (and regularise the optimisation), we solved at each iteration  $\Delta P = 0$ , where  $P = d_{zone}$  and has its estimated value fixed for the barycentre of each zone (similarly as what is done in [25]).

2) *Personalisation of Action Potential Duration*: APD for a single heart cycle is defined by the model as

$$APD_{max} = \tau_{close} \ln \left( \frac{1}{h_{min}} \right) \quad \text{where } h_{min} = 4 \left( \frac{\tau_{in}}{\tau_{out}} \right) \quad (9)$$

Here we again have one feature dependent on three parameters. We chose to estimate  $\tau_{close}$ , while keeping the others to their standard values because the Table I shows that  $\tau_{close}$  has no sensitivity to DT, whereas  $\tau_{in}$  and  $\tau_{out}$  do have. Thus estimation of  $\tau_{close}$  does not affect the adjustment of CV done before. The defined relationship (Eq 9) remains valid also in 3D thus allowing us to directly estimate  $\tau_{close}$  locally at each vertex without model simulations. The relationship is given as

$$\forall i \in S : \tau_{close}^i = APD_i^{msd} \{ \ln(\tau_{out}/4\tau_{in}) \}^{-1} \quad (10)$$

where  $APD_i^{msd}$  is the measured APD for the vertex  $i$  belonging to the surface  $S$  having data.

To propagate the estimated parameter values from the epicardium to the whole myocardium, we diffused them spatially, as explained in the previous section [25].

### B. Case 2: Personalisation Using Multiple PF

This case was applied to the second heart having multiple Basic Cycle Lengths (BCL). In this case, we estimated all parameters of the model in the following two steps: first we estimated the parameter set  $\theta = [\tau_{in} \tau_{out} \tau_{open} \tau_{close} d]$  using APD & CV restitution features jointly. Then we refined the adjustment of  $d$  using the isochrones for the largest BCL.

1) *Personalisation of Restitution curves*: Restitution defines the dependency of the next cycle APD (resp. CV) on the previous cycle Diastolic Interval (DI). For a constant PF  $f$ , the steady-state BCL remains constant :  $BCL = 1/f = APD + DI$  and thus  $APD - DI$  relationship remains constant. In order to observe and extract the macroscopic restitution, we need to have the heart optically imaged for multiple pacing frequencies, thus resulting in multiple BCL and multiple  $APD - DI$  pairs for a spatial point (here directly on optical data pixels, not mesh vertices). A dynamic pacing protocol [23] was used: the heart was paced with a given PF until it reaches a steady-state APD, and then the  $APD - DI$  pairs were measured. APD restitution curve for MS model is analytically derived [12] as

$$f(DI) = APD = \tau_{close} \ln \left( \frac{h(DI)}{h_{min}} \right) \quad (11)$$

where  $h(DI) = 1 - (1 - h_{min}) e^{-DI/\tau_{open}}$ . Similarly also CV restitution curve is derived [23] as:

$$g(DI) = \left( \frac{1}{4} (1 + \sqrt{1 - h_{min}/h(DI)}) - \frac{1}{2} (1 - \sqrt{1 - h_{min}/h(DI)}) \right) \sqrt{\frac{2dh(DI)}{\tau_{in}}} \quad (12)$$

with  $g(DI) = CV$  as the next cycle CV. Parameter  $d$  in Eq 12 has units as  $cm^2/ms$  [26], which was then converted to  $s^{-1}$  with division by  $0.1l^2$ , where  $l$  is the maximum length of the heart domain in  $m$ . From Eq 11 & Eq 12, we can observe parameter ratio ( $h_{min}$ ) controlling both APD & CV restitution. This shows a coupling between both restitutions. Thus we chose to estimate the parameters for CV restitution ( $h_{min}, \tau_{in}, d$ ) and APD restitution ( $h_{min}, \tau_{open}, \tau_{close}$ ) in a joint manner, by having a cost function  $C_r$  which minimises the error on both restitution curves and is given as,  $\forall i \in D$  :

$$\min_{\theta} \sum_{j=1}^N ((f(DI^{i,j}, \theta^i) - APD^{i,j})^2 + (g(DI^{i,j}, \theta^i) - CV^{i,j})^2) \quad (13)$$

with pixel  $i$  in the optical data  $D$  having measures,  $N$  as total number of frequency datasets,  $f(DI^{i,j}, \theta)$  corresponds to Eq 11,  $g(DI^{i,j}, \theta)$  corresponds to Eq 12 and  $\theta^i = [\tau_{close}, h_{min}, \tau_{open}, \tau_{in}, d]$  as the estimated parameter vector.  $\theta^i$  was estimated locally for each pixel  $i$  having measures for at least three different frequencies. Then a mean value for each AHA zone was computed and set to its barycentre and diffused to have smooth parameter maps. The parameter optimisation method used here is a bound-constrained active set algorithm, which uses a sequential quadratic programming method [27]. The bound set for parameters  $h_{min}, \tau_{open}, \tau_{in}$  and  $\tau_{close}$  was  $[0,1]$  (s), and for  $d$  was  $[0.1,5]$  ( $s^{-1}$ ). Parameter  $\tau_{out}$  could be estimated from estimated  $h_{min}$  &  $\tau_{in}$  using Eq 9.

2) *Personalisation of DT Isochrones*: In this step 2, we refined the estimation of parameter  $d$  for a single cycle at the lowest PF, since it represents the asymptotic value of CV restitution curve. This was done in order to have  $d$  take into account changes in CV due to the wavefront curvature on the volumetric mesh. Step 2 of this case was achieved similarly to step 1 in case 1, see Section IV-A1.

## V. RESULTS

The two datasets used here were healthy *ex-vivo* hearts. Before personalisation of the model, the simulations were computed with parameters at their standard values. Detailed quantitative results are presented in Table II, we only describe here one case of each personalisation.

### A. DT & APD error maps

For the dataset 1B-LV-Epi-r, before personalisation, the mean absolute error on the DT was 100 ms ( $\approx 58\%$  of depolarisation duration  $\approx 170$  ms), see Fig 5. It had first reduced to 59 ms ( $\approx 30\%$ ) using the calibration step for the  $d^{global}$  estimation (Fig. 5a), and then to 5 ms ( $\approx 2\%$ ) with iterative adjustment (Fig. 5b). Around 25 direct model simulations were performed for the iterative adjustment step.

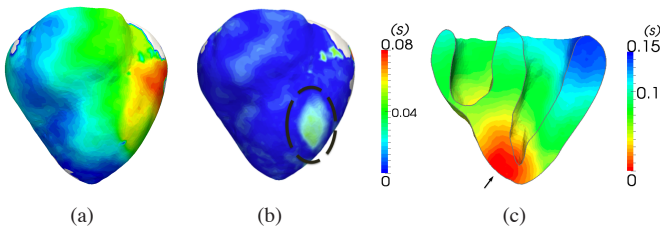


Fig. 5. DT error maps after calibration (left) and after iterative adjustment (middle) steps of personalisation in case 1 for LV-Epi-r pacing (black arrow). Black ellipse highlights the error in the low conductivity region. (Right) simulated personalised volumetric DT isochrones<sup>†</sup>.

The resulting parameter map (Fig 8.a) shows the capture of the low conductivity region (black ellipse) observed in the dataset (Fig 3). With the personalisation of parameter  $\tau_{close}$ , APD errors were reduced from 77 ms ( $\approx 25\%$  of APD  $\approx 300$ ms) before personalisation to 9 ms ( $\approx 3\%$ ), for Dataset 1C-LV-Endo. Fig 5c also shows the simulated volumetric DT isochrones after personalisation.

### B. Fitting of restitution curves

Personalisation case 2 was applied to dataset 2. The estimated parameters were  $\tau_{open}$ ,  $\tau_{close}$ ,  $\tau_{in}$ ,  $\tau_{out}$  and  $d$  using multiple pacing frequencies (Fig 6).

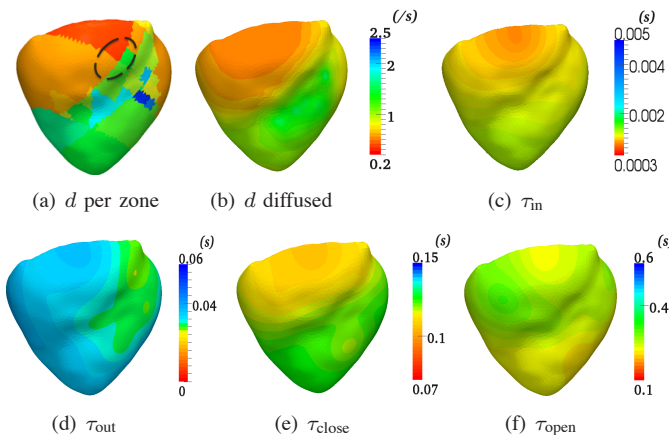


Fig. 6. Estimated parameter values on the bi-ventricular mesh using personalisation case 2. Black ellipse represent capture of low conductivity regions (Fig 3(2A-0.5Hz CV maps)).

The absolute mean square error  $C_r$  (Eq 13) was 20.35 before personalisation, and reduced to 0.54 after personalisation, which implies a good fit of the both APD and CV restitution curves to the data (Fig 7). Nonetheless as the parameters were optimised by minimising the joint error on APD and CV restitution, we can still observe some CV restitution misfits for few pixels at low frequency.

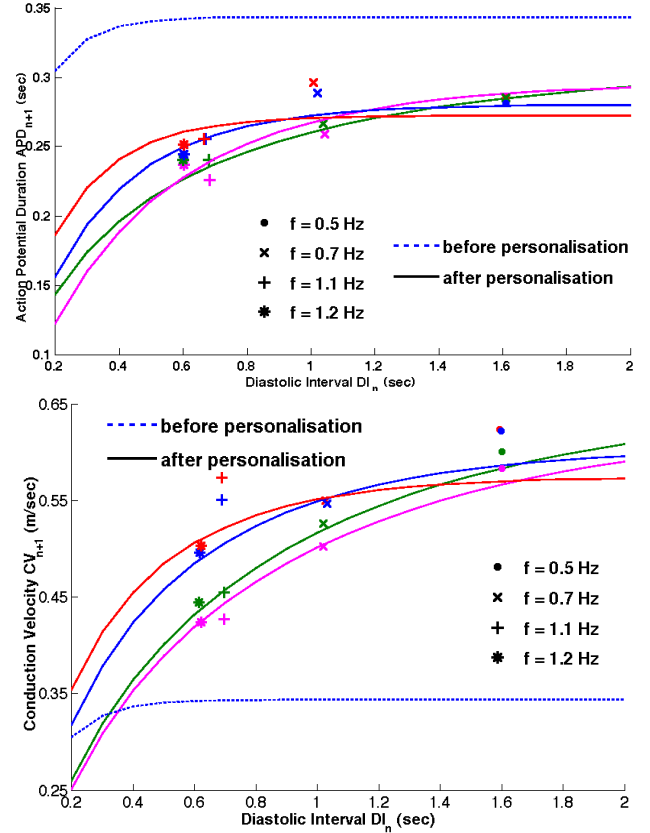


Fig. 7. Fitting of model APD (top) and CV (bottom) restitution curves to the data points extracted from dataset 2 optical data. Red, Blue, Green and Magenta colours each represent a data point.

The zonal parameters estimated showed clear differences in values of  $\tau_{in}$  &  $\tau_{out}$  for LV and RV.  $\tau_{close}$  shows lower values at the pacing location and RV zones, thus showing APD heterogeneity between the LV and RV.  $\tau_{open}$ , a parameter controlling the APD restitution slope, shows lower values (flat slope) near the pacing and basal regions compared to the remaining epicardium. The parameters depicting the tissue conductivity from the diffusion term ( $d$ ) and reaction term ( $\tau_{in}$ ), were also able to locate the low conductivity area observed in the dataset 2 (see black ellipse in Fig 3).

### C. Robustness to Pacing Location

We personalised the model with two different pacing scenarios for the same heart: LV epicardium (right side) and LV endocardium. As the personalisation is performed on the same heart at the same pacing frequency, we expect similar

<sup>†</sup>A video on model simulation without/with personalisation for 1B-LV-Epi-r pacing is available as supplementary material at <http://ieeexplore.ieee.org>

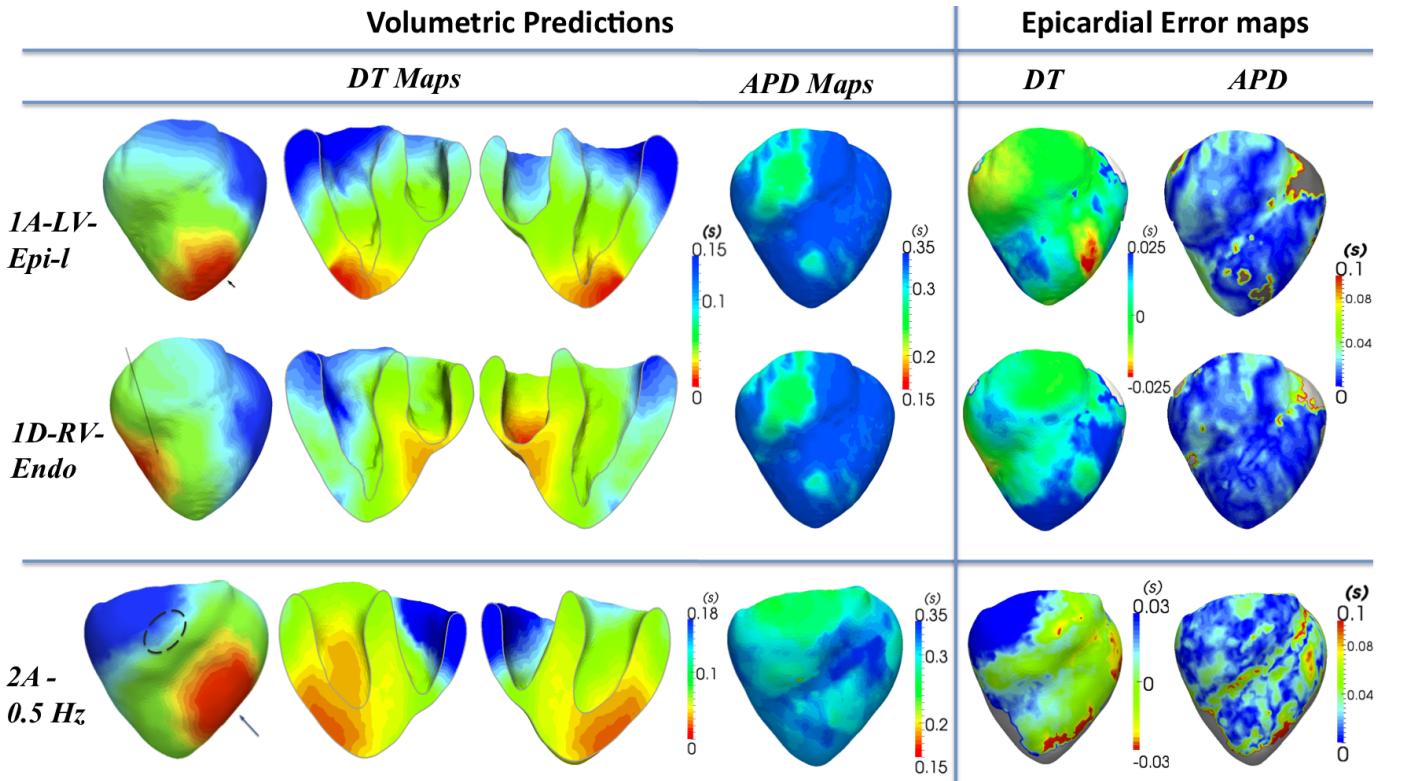


Fig. 9. Volumetric predictions using the model personalised with LV-Endo pacing for dataset 1 and with multiple PF and LV-Epi pacing for dataset 2. First row: pacing location 1A-LV-Epi-l. Second row: 1D-RV-Endo (arrows). Third row: LV-Epi, PF: 0.5Hz. First three columns: predicted volumetric DT maps, second: predicted APD maps. Please refer to Fig 3 for experimental epicardial values. Third column: DT Error maps of prediction against experimental epicardial data, fourth: APD error maps<sup>‡</sup>.

intrinsic parameters. Fig 8 and Table II show qualitative and quantitative comparison of the estimated parameter  $d$  and  $\tau_{close}$  for both pacing locations. We can observe that the parameter

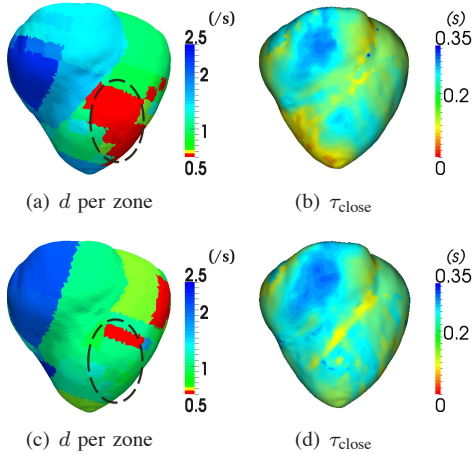


Fig. 8. Parameter maps for LV-Endo (first row) and LV-Epi-r (second row) pacing locations. Estimated  $d$  values per zone after personalisation case 1 (first column) both capture the low conductivity region (black ellipse). The second column is the estimated  $\tau_{close}$  in both cases.

values were mostly similar for both pacing locations, with the same spatial distribution and RV / LV differentiation. The low conductivity area was more basal for endocardial pacing as probably the fast conduction system is recruited. The locally estimated parameter  $\tau_{close}$  was very similar for both pacing

locations. This analysis does confirm the low sensitivity of the estimated parameter values to different pacing locations. Using Epi- & Endocardial pacing locations for such analysis also tests the capture of transmural wave propagation, when the dataset used to personalise is only epicardial surface data.

#### D. Evaluation of Volumetric Predictions

We evaluated volumetric predictions of the MS model for different pacing scenarios, using the parameters estimated from the personalisation using endocardial pacing (LV-Endo). The validation of the prediction was done in terms of the DT and APD error qualitatively (see Fig 9) and quantitatively (see Table II).

Even if the predicted isochrones produce higher errors than those produced for LV-Endo, it was still small compared to the errors obtained with standard parameters (less than 10%).

These predictions also allow to evaluate the capture of the transmural wave propagation by comparing the predicted epicardial isochrones with the measured ones. The behaviour of the model reproduces quite well the observations.

## VI. DISCUSSION

### Robustness to Pacing Location

Personalisation case 1 was able to recover approximately the same model parameters irrespective of the pacing scenar-

<sup>‡</sup>Videos of model predictions for 1A-LV-Epi-l & 1D-RV-Endo pacings are available as supplementary material at <http://icexplorer.ieee.org>

ios. The results look qualitatively and quantitatively similar (Fig 5, Fig 8 & Table II), implying low sensitivity of the personalisation framework to pacing locations. The personalisation framework was probably able to sufficiently capture the global minima of the cost function, as local minima are highly unlikely to be the same for different pacing scenarios. This also shows that the model parameters actually do not vary with different pacing locations for a single pacing frequency. However the pacing locations considered here were all near the apical regions of the endo- and epicardium. In order to have more evaluation on its robustness, we need to perform personalisations with pacing locations in the mid and basal regions, as well as with data having normal sinus rhythm conduction pathway. The fast conduction pathways can make the adjustment from epicardial data difficult because the depolarisation wave can reach the epicardial surface quite simultaneously.

#### *Estimation of Restitution Properties*

Personalisation case 2 was able to estimate all model parameters including APD and CV restitutions and can predict isochrones similar to the measured data for multiple frequencies. Restitution properties of the cardiac tissue play a crucial role in the cause of arrhythmias, hence were required to be estimated. However, in the described case 2, we estimated the parameter vector  $\theta$  and then used the estimated  $d$  as an initial guess in step 2, to refine the  $d$  estimation with DT isochrones. This second step can potentially modify the CV restitution adjustments done previously in step 1. Thus the future work would be to adjust the parameters using CV restitution and DT isochrones simultaneously.

#### *Transmural Parameters & Volumetric Prediction*

We estimated the model parameters for a volumetric mesh based on observations on the epicardial surface. But ideally, we should check our estimated parameters against measured transmural recordings. This could not be performed in this case on the *ex-vivo* heart as it damages the heart muscle, making retrieval of the fibre orientation information using DT-MRI not possible. An other option is to acquire simultaneous endocardial and epicardial data. This could be possible with catheter based mapping systems used in the clinics.

#### *Performance*

On a 2.16 GHz, dual core, 2.0 GB Intel Centrino Duo PC, the computational time of one time step for the MS model on 3D bi-ventricular mesh ( $\approx 247250$  tetrahedra) for semi-implicit MCNAB scheme was  $\approx 1$  s, with  $\delta t = 0.1$  ms and mean edge length  $\delta x = 1.5$  mm. Parameter estimation of  $d$  using DT isochrones involved  $20 \sim 30$  iterations, using simulations until the depolarisation of whole ventricles  $\approx 150$  ms. This needs a computational time of  $\approx 1500s \times n$ , where  $n$  is the number of iterations. On the other hand, parameter estimation using other features such as APD and restitution curves does not involve model simulations, but is solved using explicit analytical formulae and requires inexpensive amount

of time ( $\approx 1$  min). Thus the most time consuming part of both personalisation frameworks is the parameter estimation of  $d$ . This is due to the direct simulations of the biophysical MS model, which has a fast upstroke ( $(du/dt)_{max}$ ), thus requires very fine spatial and temporal resolutions.

#### *Study Limitations & Error sources*

On the data processing part, one of the limitations of this study was the lack of correction of the optical signals, which are quite complex and contain information from the sub-epicardial layer [28], [29]. Such corrections would give more reliable data and could improve the correspondence between the simulations and experiment, as the simulations are volumetric. However, we don't use the optical signal value as such, but we only extract depolarisation and repolarisation time-points from the data. This was extracted after filtering the data at each pixel, to constitute the DT and APD maps. We most probably get some smoothing of these maps due to the sub-epicardial layers, but we don't expect these to create major changes in the presented results as the induced error is probably small with respect to all the different error sources listed below and the resolution used.

The error sources in personalisation and prediction include: (i) Less accurate predictive power of the model due to its low complexity, (ii) Lack of successful reproducibility of transmural parameter variation due to the usage of only epicardial data. We hypothesise that these juvenile pigs do not have transmural variations, (iii) Insufficiency in modelling the actual Purkinje system, and its potential retrograde activation. However, there was no evidence from the presented data, (iv) Insufficiency of domain decomposition to reproduce accurately the spatial variation of the parameters.

#### *Application to Pathological Cases & Clinical Data*

This work can be applied to clinical data by replacing the surface optical data with surface epi- or endocardial electro-anatomical mapping of the patient. Most of the challenge lies in the reliable extraction of features such as DT and RT from sparse and noisy patient data consisting of extracellular potentials. Also the *in-vivo* acquisition of fibre orientations is challenging due to the heart motion. Nevertheless the personalisation framework can be performed using the rule-based fibre orientation, and still provides promising results [30]. Personalisation case 1 would prove to be more efficient for predictions at a constant pacing frequency as it is the case in Cardiac Resynchronisation Therapy (CRT). On the contrary, case 2 would be more preferred for arrhythmias as it can reveal more features such as APD and CV restitution properties for healthy, scars and grey zones. Also, an evaluation on the level of complexity required for simulating arrhythmias in pathological cases is needed. However, additional complexity has a strong impact on the tractability [31] and on the parameters identifiability [32].

## VII. CONCLUSION

We presented a novel method for estimating *volumetric* model parameters from *surface* data with single and multiple

Pacing Location	Parameter $d \pm \sigma$ ( $s^{-1}$ )		DT Error $\Delta \pm \sigma$ (ms)	Parameter $\tau_{close} \pm \sigma \times 10^{-4}$ (ms)		APD Error $\Delta \pm \sigma$ (ms)
	LV	RV		LV	RV	
LV-Endo	$0.95 \pm 0.03$	$1.36 \pm 0.16$	$4.22 \pm 6.75$	$0.22 \pm 1.25$	$0.20 \pm 4.90$	$4.98 \pm 8.89$
LV-Epi-r	$0.96 \pm 0.03$	$1.38 \pm 0.11$	$2.54 \pm 5.12$	$0.22 \pm 3.04$	$0.21 \pm 6.81$	$4.73 \pm 5.57$
LV-Epi-l	-	-	$12.16 \pm 14.57$	-	-	$8.62 \pm 9.21$
RV-Endo	-	-	$17.21 \pm 18.15$	-	-	$7.32 \pm 8.97$

TABLE II  
PARAMETERS AND ERRORS ( $\Delta$ : MEAN,  $\sigma$ : STANDARD DEVIATION) FOR CASE 1 PERSONALISATION (1ST ROW) AND PREDICTION (2ND ROW).

pacing frequencies. We extracted features such as CV, APD, CV and APD restitution macroscopically from the measured cardiac data and used them to personalise the model. We estimated all the model parameters making the model heart-specific. We evaluated the sensitivity of the personalisation to different epi- and endocardial pacing scenarios and the results show a robust behaviour of the framework to pacing location. Then we also tested the volumetric prediction ability of the model for different pacing scenarios and showed promising results.

#### ACKNOWLEDGMENT

This research received funding from the European Community's Seventh Framework Programme (FP7/2007-2013) under grant agreement n 224495 (euHeart project).

#### REFERENCES

- [1] A. Hodgkin and A. Huxley, "A quantitative description of membrane current and its application to conduction and excitation in nerve," *The Journal of physiology*, vol. 117, no. 4, p. 500, 1952.
- [2] D. Noble, A. Varghese, P. Kohl, and P. Noble, "Improved guinea-pig ventricular cell model incorporating a diadic space, IKr and IKs, and length- and tension-dependent processes." *The Canadian journal of cardiology*, vol. 14, no. 1, p. 123, 1998.
- [3] J. Keener, J. Keener, and J. Sneyd, *Mathematical physiology: Cellular physiology*. Springer Verlag, 2009.
- [4] K. Ten Tusscher, D. Noble, P. Noble, and A. Panfilov, "A model for human ventricular tissue," *American Journal of Physiology- Heart and Circulatory Physiology*, vol. 286, no. 4, p. H1573, 2004.
- [5] G. Beeler and H. Reuter, "Reconstruction of the action potential of ventricular myocardial fibres," *The Journal of physiology*, vol. 268, no. 1, p. 177, 1977.
- [6] C. Luo and Y. Rudy, "A model of the ventricular cardiac action potential. depolarization, repolarization, and their interaction," *Circulation Research*, vol. 68, no. 6, p. 1501, 1991.
- [7] P. Colli Franzone, L. Guerri, M. Pennacchio, and B. Taccardi, "Spread of excitation in 3-D models of the anisotropic cardiac tissue. II. Effects of fiber architecture and ventricular geometry," *Mathematical biosciences*, vol. 147, no. 2, pp. 131–172, 1998.
- [8] M. Sermesant, E. Konukoglu, H. Delingette, Y. Coudiere, P. Chinchapatnam, K. Rhode, R. Razavi, and N. Ayache, "An anisotropic multi-front fast marching method for real-time simulation of cardiac electrophysiology," vol. 4466 of LNCS. Springer, 2007, pp. 160–169.
- [9] R. Fitzhugh, "Impulses and physiological states in theoretical models of nerve membrane," *Biophysical Journal*, vol. 1, no. 6, pp. 445–466, 1961.
- [10] R. R. Aliev and A. V. Panfilov, "A simple two-variable model of cardiac excitation," *Chaos, Solitons & Fractals*, vol. 7, no. 3, pp. 293–301, 1996.
- [11] O. Bernus, R. Wilders, C. Zemlin, H. Vershelde, and A. Panfilov, "A computationally efficient electrophysiological model of human ventricular cells," *American Journal of Physiology- Heart and Circulatory Physiology*, vol. 282, no. 6, p. H2296, 2002.
- [12] C. Mitchell and D. Schaeffer, "A two-current model for the dynamics of cardiac membrane," *Bulletin of mathematical biology*, vol. 65, no. 5, pp. 767–793, 2003.
- [13] J. Relan, M. Sermesant, H. Delingette, M. Pop, G. Wright, and N. Ayache, "Quantitative comparison of two cardiac electrophysiology models using personalisation to optical and MR data," in *Biomedical Imaging: From Nano to Macro, 2009. ISBI'09. IEEE International Symposium on*. IEEE, 2009, pp. 1027–1030.
- [14] M. Pop, M. Sermesant, D. Lepiller, M. Truong, E. McVeigh, E. Crystal, A. Dick, H. Delingette, N. Ayache, and G. Wright, "Fusion of optical imaging and MRI for the evaluation and adjustment of macroscopic models of cardiac electrophysiology: A feasibility study," *Medical Image Analysis*, vol. 13, no. 2, pp. 370–380, 2009.
- [15] V. Moreau-Villéger, H. Delingette, M. Sermesant, H. Ashikaga, E. McVeigh, and N. Ayache, "Building maps of local apparent conductivity of the epicardium with a 2-D electrophysiological model of the heart," *Biomedical Engineering, IEEE Transactions on*, vol. 53, no. 8, pp. 1457–1466, 2006.
- [16] P. Chinchapatnam, K. Rhode, M. Ginks, C. Rinaldi, P. Lambiase, R. Razavi, S. Arridge, and M. Sermesant, "Model-based imaging of cardiac apparent conductivity and local conduction velocity for diagnosis and planning of therapy," *Medical Imaging, IEEE Transactions on*, vol. 27, no. 11, pp. 1631–1642, 2008.
- [17] D. Lepiller, M. Sermesant, M. Pop, H. Delingette, G. Wright, and N. Ayache, "Cardiac electrophysiology model adjustment using the fusion of MR and optical imaging," vol. 5241 of LNCS. Springer, 2008, pp. 678–685.
- [18] I. Efimov, V. Nikolski, and G. Salama, "Optical imaging of the heart," *Circulation research*, vol. 95, no. 1, p. 21, 2004.
- [19] D. Chung, M. Pop, M. Sermesant, and G. Wright, "Stereo reconstruction of the epicardium for optical fluorescence imaging," in *MICCAI Workshop on Biophotonics for diagnosis and treatment. IMM-Technical Report*, 2006, pp. 33–40.
- [20] F. Fenton and A. Karma, "Vortex dynamics in three-dimensional continuous myocardium with fiber rotation: filament instability and fibrillation," *Chaos*, vol. 8, no. 1, pp. 20–47, 1998.
- [21] M. Sermesant, H. Delingette, and N. Ayache, "An electromechanical model of the heart for image analysis and simulation," *Medical Imaging, IEEE Transactions on*, vol. 25, no. 5, pp. 612–625, 2006.
- [22] M. Ethier and Y. Bourgault, "Semi-implicit time-discretization schemes for the bidomain model," *SIAM Journal on Numerical Analysis*, vol. 46, p. 2443, 2008.
- [23] J. Cain, E. Tolkacheva, D. Schaeffer, and D. Gauthier, "Rate-dependent propagation of cardiac action potentials in a one-dimensional fiber," *Physical Review E*, vol. 70, no. 6, pp. 061906–1–061906–7, 2004.
- [24] A. Conn, N. Gould, and P. Toint, *Trust-region methods*. Society for Industrial Mathematics, 2000.
- [25] R. Keldermann, K. Ten Tusscher, M. Nash, R. Hren, P. Taggart, and A. Panfilov, "Effect of heterogeneous apd restitution on vf organization in a model of the human ventricles," *American Journal of Physiology-Heart and Circulatory Physiology*, vol. 294, no. 2, p. H764, 2008.
- [26] J. Cain, "A kinematic model of wave propagation," 2008.
- [27] R. Fletcher and M. Powell, "A rapidly convergent descent method for minimization," *The Computer Journal*, vol. 6, no. 2, p. 163, 1963.
- [28] C. Hyatt, S. Mironov, F. Vetter, C. Zemlin, and A. Pertsov, "Optical action potential upstroke morphology reveals near-surface transmurular propagation direction," *Circulation research*, vol. 97, no. 3, p. 277, 2005.
- [29] M. Bishop, B. Rodriguez, J. Eason, J. Whiteley, N. Trayanova, and D. Gavaghan, "Synthesis of voltage-sensitive optical signals: application to panoramic optical mapping," *Biophysical journal*, vol. 90, no. 8, pp. 2938–2945, 2006.
- [30] J. Relan, P. Chinchapatnam, M. Sermesant, K. Rhode, H. Delingette, R. Razavi, and N. Ayache, "Coupled personalisation of electrophysiology models for simulation of induced ischemic ventricular tachycardia,"

- in *Medical Image Computing and Computer-Assisted Intervention—MICCAI 2010*, vol. 6362 of LNCS. Springer, 2010, pp. 420–428.
- [31] A. Garna, D. Noble, and P. Kohl, “Dimensionality in cardiac modelling,” *Progress in biophysics and molecular biology*, vol. 87, no. 1, pp. 47–66, 2005.
- [32] M. Fink and D. Noble, “Markov models for ion channels: versatility versus identifiability and speed,” *Philosophical Transactions of the Royal Society A: Mathematical, Physical and Engineering Sciences*, vol. 367, no. 1896, p. 2161, 2009.



**Jatin Relan** received his Masters of Science degree in Biomedical Engineering from Fachhochschule Lübeck and Universität zu Lübeck, Germany, in 2008. He is currently a PhD student of computer science at Ecole de Mines ParisTech, Paris, France and is working with the ASCLEPIOS research team at the INRIA research center in Sophia Antipolis, France. His PhD work is on the planning of cardiac radio-frequency ablation therapy for ventricular tachycardia and is a part of an European project euHeart: Personalised & Integrated Cardiac Care

using patient-specific cardiovascular modelling.

His research interests include biomedical image processing, computational cardiac modelling, building patient-specific cardiac electrophysiology models from clinical data analysis for diagnosis and pathology simulation such as cardiac arrhythmias for therapy planning.



**Dr. Mihaela Pop** obtained her M.Sc. in 2003 from the Department of Medical Biophysics, University of Toronto, working on characterization of dielectric properties of kidney tissue at RF ablation frequencies during heating, as well as on building computer models for treatment planning. She completed her PhD in 2010 in the same Department of Medical Biophysics, working on the construction of 3D MR image-based computer models of electrophysiology, which integrated experimental measures from optical fluorescence imaging and electro-anatomical

CARTO voltage maps. She is currently a post-doctoral fellow at Sunnybrook Research Centre (Toronto), continuing to work on the development of biophysical models and preclinical experimental models, as well as on the integration of image-guided ablative therapies into clinical platforms, with an aim to understand and predict the inducibility of arrhythmias in patients with prior myocardial infarction.



**Dr. Hervé Delingette** is currently a research director in the ASCLEPIOS research team at the INRIA research center in Sophia Antipolis. He received in 1989 a Master degree and in 1994 a PhD degree from the Ecole Centrale des Arts et Manufactures de Paris, (France) and was habilitated in 2006. From 1989 until 1992, he was a Visiting Scientist at the Robotics Institute of Carnegie Mellon University (CMU) and the Human Interface Laboratory of Nippon Telegraph and Telephone (NTT). His research interests are in the fields of medical image analysis,

image segmentation, soft tissue modelling, surgery simulation and computational models of the human body. He authored more than 60 journal papers in those fields and co-chaired the First Symposium on Surgery Simulation and Soft Tissue Modelling in 2003 and the fifth international conference on Functional Imaging and Modelling of the Heart in 2009.



**Prof. Graham A. Wright** is currently the director of the Schulich Heart Research Program at Sunnybrook Health Sciences Centre, a senior scientist at Sunnybrook Research Institute and a professor in the Department of Medical Biophysics at the University of Toronto. He was appointed the Canada Research Chair in Imaging for Cardiovascular Therapeutics, effective May 1, 2010. He also serves on the coordinating committees of the Cardiovascular Sciences Collaborative Program and the Heart and Stroke Richard Lewar Centre of Excellence respectively, at the University of Toronto. He is also a Scholar in the McLaughlin Centre for Molecular Medicine and was recently honoured as President-Elect of the International MR Angio Club.



**Prof. Nicholas Ayache** is a Research Director at INRIA Sophia Antipolis, France, where he leads the ASCLEPIOS research team. He received his Ph.D in 1983, and his “Thèse d’Etat” in 1988 from Univ. of Paris XI (Computer Science), introducing new recognition and stereovision capabilities for autonomous robots.

Since 1988, N. Ayache’s research activities have been dedicated to Computational Medical Image Analysis and Simulation applied to medicine to better assist diagnosis and therapy. His research interests include the design of novel geometrical, statistical, physical and functional models for image analysis, surgery simulation and image-guided therapy. He is the author of over 350 peer-reviewed scientific articles in these domains, the author or editor of 8 books, and the co-founder of 4 start-up companies in computer vision, computer graphics, medical and biological imaging.

N. Ayache is co-Editor in Chief (and co-founder) of the Medical Image Analysis journal (Elsevier), and associate editor of several scientific journals including IEEE Trans. Med. Imaging. He has been involved in the organization of several major and pioneering conferences in the field including MICCAI (Medical Image Computing and Comp. Assist. Intervention). He was an invited scientist at MIT and Harvard (Boston) for a semester in 2007.

N. Ayache received prestigious awards, including the EADS Grand Prize awarded by the French Academy of Sciences in 2006 and the Microsoft Award for Science in Europe, awarded jointly by the UK Royal Society and the French Academy of Sciences in 2008.



**Dr. Maxime Sermesant** received his Diploma in General Engineering from Ecole Centrale Paris, Paris, France in 1999, his MSc from Ecole Normale Supérieure de Cachan, Cachan, France in 1999, and his PhD in Control, Signal and Image Processing from the University of Nice - Sophia Antipolis, France in 2003. From June 2003 to December 2005, he was a Research Fellow with the Cardiac MR Research Group, Guys Hospital, Kings College London, UK and since 2005, he is a Research Scientist at INRIA in the ASCLEPIOS team and a part-time

Lecturer at King’s College London, Division of Imaging Sciences, St Thomas’ Hospital. His research interests include biomedical image processing and organ modelling. The integration of these two areas open up possibilities in clinical data analysis for diagnosis, and in pathology simulation for therapy planning. His main focus in the recent years have been the application of patient-specific models of the heart to cardiac pathologies.